

A solvable model for graph state decoherence dynamics

Jérôme Houdayer^{1*}, Haggai Landa², and Grégoire Misguich¹

¹ Université Paris-Saclay, CNRS, CEA, Institut de physique théorique,
91191 Gif-sur-Yvette, France

² IBM Quantum, IBM Research – Israel, Haifa University Campus, Mount Carmel,
Haifa 31905, Israel

* jerome.houdayer@ipht.fr

May 30, 2023

Abstract

We present an exactly solvable toy model for the continuous dissipative dynamics of permutation-invariant graph states of N qubits. Such states are locally equivalent to an N -qubit Greenberger-Horne-Zeilinger (GHZ) state, a fundamental resource in many quantum information processing setups. We focus on the time evolution of the state governed by a Lindblad master equation with the three standard single-qubit jump operators, the Hamiltonian part being set to zero. Deriving analytic expressions for the expectation values of observables expanded in the Pauli basis at all times, we analyze the nontrivial intermediate-time dynamics. Using a numerical solver based on matrix product operators we simulate the time evolution for systems with up to 64 qubits and verify a numerically exact agreement with the analytical results. We find that the evolution of the operator space entanglement entropy of a bipartition of the system manifests a plateau whose duration increases logarithmically with the number of qubits, whereas all Pauli-operator products have expectation values decaying at most in constant time.

1 Introduction

Graph states were introduced by Briegel and Raussendorf in 2001 [1] as special entangled states of N qubits. These states with multipartite entanglement play an important role in quantum information theory because they can be employed as a resource in a measurement-based quantum computation framework [2, 3], they can be used in error correction codes [4] and for quantum communications [5]. In particular, permutation-invariant graph states [6], which are locally equivalent to an N -qubit Greenberger-Horne-Zeilinger (GHZ) state, are the subject of extensive research [7–10] and their creation and characterization serve as one of a few standard benchmarks of quantum computation hardware [11–13]. The use of graph states for information processing in current quantum devices will inevitably have to face uncontrolled decoherence processes and some aspects of graph state entanglement under the presence of decoherence have already been investigated [14–17]. Most of these previous works focused on discrete evolutions of the density matrix via completely positive maps (noisy channels).

In this work, we introduce and discuss a model of a graph state realized with qubits (or spin-one-half particles), which decoheres continuously in time as described by a Lindblad master equation for the density operator [18, 19]. We account for the three most prevalent local jump operators (dissipators); Two jump terms describe the incoherent transitions from $|0\rangle$ to $|1\rangle$ (and vice versa), and the third one is the so-called dephasing term. The initial state is a pure (graph) state, and it evolves into a mixed state under the action of the dissipation. Although it is a many-body problem, the structure of the model is simple enough that the expectation

values of any observable can here be computed exactly by solving the equations of motion for the expectation values of product of Pauli matrices.

We complement our analytic treatment with the use of a numerical Lindblad solver [20, 21], which is internally based on the C++ ITensor library [22] (see also [23] for a review on available numerical methods for this type of problem). In the solver, the state of the system – a many-body density matrix ρ – is stored in the form a matrix-product operator (MPO). Since ρ is in general a matrix of size $2^N \times 2^N$, a brute-force numerical simulation of the Lindblad dynamics generally becomes very demanding beyond a dozen of qubits. Taking advantage of the fact that the states produced along the time evolution are only mildly correlated in the present model, the MPO approach allows us to reach a very high accuracy with modest computing resources (i.e. low MPO bond dimension) even with as many as $N = 64$ qubits. Other numerical approaches would also be efficient in the context of the current setup [6, 24].

The presented model can be viewed as a toy model illustrating the basic mechanisms at play and gaining an understanding of the dominant dynamical behavior in similar setups. It may also be used as a starting point for more realistic studies with different graph states and some Hamiltonian terms competing with the dissipators. With our numerical approach we are able to calculate global quantities that are not immediately accessible analytically, and observe an interesting scaling with size of bipartite correlations in the system.

2 Notations and definition of the model

We consider a system composed of N qubits (with basis states $|0\rangle = |\uparrow\rangle$ and $|1\rangle = |\downarrow\rangle$), indexed with $i = 1 \dots N$. We denote the usual Pauli operators by σ^x , σ^y and σ^z , or alternatively by X , Y and Z . Additionally, we define $\sigma^\pm = \frac{1}{2}(\sigma^x \pm i\sigma^y)$.

For completeness, we start by recalling the definition of a graph state. A graph state is an entangled state that can be produced by the symmetrical 2-qubit gate “controlled-Z” (CZ), which is defined by its matrix

$$CZ = \begin{pmatrix} 1 & 0 & 0 & 0 \\ 0 & 1 & 0 & 0 \\ 0 & 0 & 1 & 0 \\ 0 & 0 & 0 & -1 \end{pmatrix} \quad (1)$$

in the basis $\{|00\rangle, |10\rangle, |01\rangle, |11\rangle\}$. Given an undirected graph $G(V, E)$ where $V = 1 \dots N$ represents the qubits and $E \subset V \times V$ is the set of edges, the corresponding graph state $|g\rangle$ is defined by

$$|g\rangle = \prod_{(i,j) \in E} CZ(i, j) |+\dots+\rangle, \quad (2)$$

where $|+\rangle = \frac{1}{\sqrt{2}}(|0\rangle + |1\rangle)$. It is well known [1], that the graph state $|g\rangle$ is characterized by its stabilizers

$$S_i = \sigma_i^x \prod_{j|(i,j) \in E} \sigma_j^z, \quad (3)$$

through

$$S_i |g\rangle = |g\rangle. \quad (4)$$

In the present study, we focus on the case where the system is *invariant under any permutation of the N qubits*. We start at $t = 0$ from the only non-trivial fully symmetrical graph state, that is the graph state associated to the complete graph. A complete graph is a graph where all possible edges are present, so that each vertex is linked to the $N - 1$ other vertices. Our

initial state (at $t = 0$) is thus given by

$$|g\rangle = \prod_{i<j} CZ(i, j) |++\cdots+\rangle, \quad (5)$$

As a side remark we note that, thanks to the transformation rules of graph states under the action of local Clifford (LC) gates [15], the complete graph is LC-equivalent to the star graph.¹ In turn, the star graph state can be transformed into the N -qubit Greenberger-Horne-Zeilinger (GHZ) state [25] by application of Hadamard gates to all qubits except the center of the star. The complete graph is thus LC-equivalent to the GHZ state.

We consider a time evolution generated by a Lindblad equation (see for example [26]) where the Hamiltonian part is set to zero. The state of the system is described by its density matrix ρ whose time evolution is given by

$$\frac{\partial}{\partial t} \rho = \mathcal{D}[\rho], \quad (6)$$

where \mathcal{D} is the dissipator, a linear superoperator acting on ρ . We consider three possible terms in the dissipator $\mathcal{D} = \mathcal{D}_0 + \mathcal{D}_1 + \mathcal{D}_2$. They are given by

$$\mathcal{D}_0[\rho] = g_0 \sum_i \left(\sigma_i^+ \rho \sigma_i^- - \frac{1}{2} \{ \sigma_i^- \sigma_i^+, \rho \} \right), \quad (7)$$

$$\mathcal{D}_1[\rho] = g_1 \sum_i \left(\sigma_i^- \rho \sigma_i^+ - \frac{1}{2} \{ \sigma_i^+ \sigma_i^-, \rho \} \right). \quad (8)$$

$$\mathcal{D}_2[\rho] = g_2 \sum_i (\sigma_i^z \rho \sigma_i^z - \rho). \quad (9)$$

where $\{, \}$ is the anticommutator.² \mathcal{D}_0 (resp. \mathcal{D}_1) then corresponds to an incoherent transition toward the state $|0\rangle$ (resp. $|1\rangle$). \mathcal{D}_2 corresponds to a dephasing in the xy -plane.

In the next section, we show how to compute exactly the evolution of the expectation value of any product of Pauli matrices in this model. From this result one can then obtain the expectation value of any observable as a function of time. In Sec. 4, we will then compare these analytical results with numerical simulations based on a matrix product operator (MPO) representation of the density matrix. Sec. 5 provides some concluding remarks.

3 Closed-form observable dynamics

3.1 Observable dynamics

To compute the evolution of the mean value of a given (time-independent) observable O , we start from the fact that $\langle O \rangle = \text{Tr}(\rho O)$ and we use Eq. 6 to get

$$\begin{aligned} \frac{\partial}{\partial t} \langle O \rangle &= \frac{\partial}{\partial t} \text{Tr}(\rho O) = \text{Tr} \left(\frac{\partial \rho}{\partial t} O \right) \\ &= \text{Tr}(\mathcal{D}[\rho] O) \\ &= \text{Tr}(\mathcal{D}_0[\rho] O) + \text{Tr}(\mathcal{D}_1[\rho] O) + \text{Tr}(\mathcal{D}_2[\rho] O). \end{aligned} \quad (10)$$

¹The star graph has a central vertex connected to all the other vertices.

² $\{A, B\} = AB + BA$.

First let us consider \mathcal{D}_0

$$\begin{aligned}\mathrm{Tr}(\mathcal{D}_0[\rho]O) &= g_0 \sum_i \mathrm{Tr} \left[(\sigma_i^+ \rho \sigma_i^- - \frac{1}{2} \{ \sigma_i^- \sigma_i^+, \rho \}) O \right] \\ &= g_0 \sum_i \mathrm{Tr} \left[\rho \left(\sigma_i^- O \sigma_i^+ - \frac{1}{2} \{ \sigma_i^- \sigma_i^+, O \} \right) \right] \\ &= g_0 \sum_i \langle \Lambda_0^i [O] \rangle,\end{aligned}\tag{11}$$

where the superoperator Λ_0^i is given by

$$\Lambda_0^i [O] = \sigma_i^- O \sigma_i^+ - \frac{1}{2} \{ \sigma_i^- \sigma_i^+, O \}.\tag{12}$$

Similarly, we have

$$\mathrm{Tr}(\mathcal{D}_1[\rho]O) = g_1 \sum_i \langle \Lambda_1^i [O] \rangle,\tag{13}$$

$$\mathrm{Tr}(\mathcal{D}_2[\rho]O) = g_2 \sum_i \langle \Lambda_2^i [O] \rangle,\tag{14}$$

with

$$\Lambda_1^i [O] = \sigma_i^+ O \sigma_i^- - \frac{1}{2} \{ \sigma_i^+ \sigma_i^-, O \},\tag{15}$$

$$\Lambda_2^i [O] = \sigma_i^z O \sigma_i^z - O.\tag{16}$$

It is clear that if O does not operate on qubit i then $\Lambda_*^i [O] = 0$. Moreover, for an operator O_i acting on qubit i only, $\Lambda_*^i [O_i]$ commutes with operators acting on the other qubits. The nontrivial action of the Λ_*^i can then be summarized by the following relations:

$$\begin{array}{lll}\Lambda_0[\sigma^x] = -\frac{1}{2}\sigma^x & \Lambda_1[\sigma^x] = -\frac{1}{2}\sigma^x & \Lambda_2[\sigma^x] = -2\sigma^x \\ \Lambda_0[\sigma^y] = -\frac{1}{2}\sigma^y & \Lambda_1[\sigma^y] = -\frac{1}{2}\sigma^y & \Lambda_2[\sigma^y] = -2\sigma^y \\ \Lambda_0[\sigma^z] = 1 - \sigma^z & \Lambda_1[\sigma^z] = -1 - \sigma^z & \Lambda_2[\sigma^z] = 0,\end{array}$$

where the qubit index of the Pauli operators are identical in the l.h.s and r.h.s and have been omitted for brevity.

3.2 Observables at $t = 0$

To lighten the notations, we will write X_i instead of σ_i^x and likewise for Y and Z . As our system is invariant under any permutation of the qubits, specific indices are irrelevant. In the following, we will note $\langle X \rangle = \langle \sigma_i^x \rangle$ and likewise for $\langle Y \rangle$ and $\langle Z \rangle$. More generally, we note $\langle X^n Y^m Z^l \rangle = \langle \sigma_1^x \dots \sigma_n^x \sigma_{n+1}^y \dots \sigma_{n+m}^y \sigma_{n+m+1}^z \dots \sigma_{n+m+l}^z \rangle$ which is independent of the actual order of the operators or the specific indices as long as they are all different. When indices are necessary, we will add them, for example $\langle X_1 Z_1 Y^2 Z \rangle$ is the same as $\langle X_1 Z_1 Y_2 Y_3 Z_4 \rangle$. Likewise, $\langle (X_i Z_i)^2 (Y_j X_j)^2 Z \rangle$ is the same as $\langle X_1 Z_1 X_2 Z_2 Y_3 X_3 Y_4 X_4 Z_5 \rangle$.

To compute the expectation value of a product of Pauli operators at $t = 0$, that is on the complete graph state $|g\rangle$, we start with two remarks. First the stabilizer $S = XZ^{N-1}$ leaves $|g\rangle$ unchanged (see Eqs. 3 and 4) so that

$$\langle XZ^{N-1} \rangle = \langle g | XZ^{N-1} | g \rangle = \langle g | g \rangle = 1.\tag{17}$$

Second, since Z commutes with CZ and since $CZ^2 = 1$, we have for $n > 0$

$$\begin{aligned}
\langle Z^n \rangle &= \langle g | Z^n | g \rangle \\
&= \langle + \cdots + | Z^n | + \cdots + \rangle \\
&= \langle + \cdots + | - \cdots - + \cdots + \rangle \\
&= 0.
\end{aligned} \tag{18}$$

We start by computing observables of the form $\langle X^n Z^l \rangle$. To do this, we introduce the stabilizer at one of the indices of the X . So for $n > 0$

$$\begin{aligned}
\langle X^n Z^l \rangle &= \langle X_1 X^{n-1} Z^l X_1 Z^{N-1} \rangle \\
&= \langle (X_i Z_i)^{n-1} Z^{N-l-n} \rangle \\
&= (-i)^{n-1} \langle Y^{n-1} Z^{N-l-n} \rangle \\
&= (-1)^{\frac{n-1}{2}} \langle Y^{n-1} Z^{N-l-n} \rangle.
\end{aligned} \tag{19}$$

To be real, this of course must be 0 when n is even. We can do the same for $\langle Y^m Z^l \rangle$, which gives for $m > 0$

$$\begin{aligned}
\langle Y^m Z^l \rangle &= \langle Y_1 Y^{m-1} Z^l X_1 Z^{N-1} \rangle \\
&= \langle Y_1 X_1 (Y_i Z_i)^{m-1} Z^{N-l-m} \rangle \\
&= i^{m-2} \langle X^{m-1} Z^{N-l-m+1} \rangle \\
&= (-1)^{\frac{m}{2}-1} \langle X^{m-1} Z^{N-l-m+1} \rangle.
\end{aligned} \tag{20}$$

And again this must be 0 if m is odd. Substituting Eq. 19 in Eq. 20, we can conclude that for even m

$$\langle Y^m Z^l \rangle = \langle Y^{m-2} Z^l \rangle = \langle Z^l \rangle, \tag{21}$$

which is 0 if $l > 0$ and 1 otherwise. We can also finish the computation for X for odd n

$$\begin{aligned}
\langle X^n Z^l \rangle &= (-1)^{\frac{n-1}{2}} \langle Y^{n-1} Z^{N-l-n} \rangle \\
&= (-1)^{\frac{n-1}{2}} \langle Z^{N-l-n} \rangle,
\end{aligned} \tag{22}$$

which is 1 if $n+l = N$, and zero otherwise. The last product we have not yet computed is the general one $\langle X^n Y^m Z^l \rangle$ with $n > 0$ and $m > 0$.

$$\begin{aligned}
\langle X^n Y^m Z^l \rangle &= \langle X_1 X^{n-1} Y^m Z^l X_1 Z^{N-1} \rangle \\
&= \langle (X_i Z_i)^{n-1} (Y_j Z_j)^m Z^{N-n-m-l} \rangle \\
&= i^{m-n+1} \langle X^m Y^{n-1} Z^{N-n-m-l} \rangle \\
&= (-1)^{\frac{m-n+1}{2}} \langle X^m Y^{n-1} Z^{N-n-m-l} \rangle.
\end{aligned} \tag{23}$$

This can be nonzero only if $n+m$ is even. But if $m = 1$ there are no Y left and this is zero according to Eq. 22. And if $m > 1$, the right-hand side can be nonzero only if $n+m-1$ is even (thus $n+m$ is odd) which we already excluded. Thus, $\langle X^n Y^m Z^l \rangle = 0$ if $n > 0$ and $m > 0$.

To summarize, only the following products of Pauli operators have nonzero mean values in the complete graph state:

$$\langle X^{2n+1} Z^{N-2n-1} \rangle = (-1)^n \quad \text{and} \quad \langle Y^{2n} \rangle = 1. \tag{24}$$

3.3 Solution of the equations of motion

We start with an example to show how the equation of motion leads to some differential equations. Here we consider $\langle XZ \rangle$ in the case where only g_0 is not zero.

$$\begin{aligned}
\frac{\partial}{\partial t} \langle XZ \rangle &= \frac{\partial}{\partial t} \langle X_1 Z_2 \rangle \\
&= \text{Tr}[\mathcal{D}_0[\rho](X_1 Z_2)] \\
&= g_0 \sum_i \langle \Lambda_0^i[X_1 Z_2] \rangle \\
&= g_0 (\langle \Lambda_0^1[X_1] Z_2 \rangle + \langle X_1 \Lambda_0^2[Z_2] \rangle) \\
&= g_0 \left(-\frac{1}{2} \langle X_1 Z_2 \rangle + \langle X_1 (1 - Z_2) \rangle \right) \\
&= g_0 \left(-\frac{3}{2} \langle XZ \rangle + \langle X \rangle \right).
\end{aligned} \tag{25}$$

Now the general formula for $\frac{\partial}{\partial t} \langle X^n Y^m Z^l \rangle$ and all dissipators: each X or Y gives a term $(-g_0/2 - g_1/2 - 2g_2) \langle X^n Y^m Z^l \rangle$ and each Z gives the two terms

$$(-g_0 - g_1) \langle X^n Y^m Z^l \rangle, \quad (g_0 - g_1) \langle X^n Y^m Z^{l-1} \rangle. \tag{26}$$

Globally, we obtain for $l > 0$

$$\frac{\partial}{\partial t} \langle X^n Y^m Z^l \rangle = -(\alpha(n+m) + \beta l) \langle X^n Y^m Z^l \rangle + \gamma l \langle X^n Y^m Z^{l-1} \rangle, \tag{27}$$

$$\frac{\partial}{\partial t} \langle X^n Y^m \rangle = -\alpha(n+m) \langle X^n Y^m \rangle, \tag{28}$$

where

$$\alpha = \frac{g_0 + g_1}{2} + 2g_2, \quad \beta = g_0 + g_1, \quad \gamma = g_0 - g_1. \tag{29}$$

Here, α is the rate of dephasing (decoherence) associated to X and Y (with its inverse equal to the characteristic T_2 timescale), β is the decay parameter associated to Z – the inverse of the relaxation time T_1 , γ is the global drive towards the steady state, and γ/β determines the thermal steady state population (value of $\langle Z \rangle$) reached in the limit of large time. In the case where $\gamma = 0$ (that is $g_0 = g_1$), all observables have a simple exponential decay.

These equations can be solved by recurrence starting at $l = 0$ using the initial conditions of the previous section. Indeed, at $l = 0$ (that is no Z), we get

$$\langle Y^{2n} \rangle = e^{-2\alpha n t}, \tag{30}$$

and all the others products without Z give zero because they start at 0 and stay there. Now we can increase l and get

$$\langle Y^{2n} Z^l \rangle = \left(\frac{\gamma}{\beta} (1 - e^{-\beta t}) \right)^l e^{-2\alpha n t}. \tag{31}$$

Note that if $\gamma = 0$ or $\gamma = \beta = 0$ then $\langle Y^{2n} Z^l \rangle = 0$ for $l > 0$. Finally, for $\langle X^{2n+1} Z^{N-2n-1} \rangle$, the equations are directly solved and we obtain

$$\langle X^{2n+1} Z^{N-2n-1} \rangle = (-1)^n e^{-((2n+1)(\alpha-\beta)+N\beta)t}, \tag{32}$$

with all the others being identically zero.

It is interesting to note that the stabilizers, that characterize the initial graph state decay very rapidly, i.e. with a timescale inversely proportional to the size of the system. This reflects some relative fragility of the graph state correlations in the present dissipative context, and may be related to the extensive number of neighbors in the initial complete graph.

3.4 Reduced density matrices

The 2-qubit density matrix can be obtained from the two-point correlations computed previously. Writing $z_{\pm} = 1 \pm \langle Z \rangle = 1 \pm \frac{\gamma}{\beta} (1 - e^{-\beta t})$ (see Eq. 31 with $n = 0$ and $l = 1$) and $y^2 = \langle YY \rangle = e^{-2\alpha t}$ (see Eq. 30 with $n = 1$), this matrix reads (for $N > 2$ only)

$$\rho_2 = \frac{1}{4} \begin{pmatrix} z_+^2 & 0 & 0 & -y^2 \\ 0 & z_+z_- & y^2 & 0 \\ 0 & y^2 & z_+z_- & 0 \\ -y^2 & 0 & 0 & z_-^2 \end{pmatrix}. \quad (33)$$

Likewise for 3 qubits and $N > 3$, we have

$$\rho_3 = \frac{1}{8} \begin{pmatrix} z_+^3 & 0 & 0 & -y^2z_+ & 0 & -y^2z_+ & -y^2z_+ & 0 \\ 0 & z_-z_+^2 & y^2z_+ & 0 & y^2z_+ & 0 & 0 & -y^2z_- \\ 0 & y^2z_+ & z_-z_+^2 & 0 & y^2z_+ & 0 & 0 & -y^2z_- \\ -y^2z_+ & 0 & 0 & z_-^2z_+ & 0 & y^2z_- & y^2z_- & 0 \\ 0 & y^2z_+ & y^2z_+ & 0 & z_-z_+^2 & 0 & 0 & -y^2z_- \\ -y^2z_+ & 0 & 0 & y^2z_- & 0 & z_-^2z_+ & y^2z_- & 0 \\ -y^2z_+ & 0 & 0 & y^2z_- & 0 & y^2z_- & z_-^2z_+ & 0 \\ 0 & -y^2z_- & -y^2z_- & 0 & -y^2z_- & 0 & 0 & z_-^3 \end{pmatrix}. \quad (34)$$

More generally, reduced density matrices for larger subsystem can be obtained by noting that each matrix element is the expectation value of a product of N operators which are of the type $(Z_i + 1)/2$ (if the matrix element connects two states where $Z_i = 1$), $(1 - Z_i)/2$ (matrix element between two states where $Z_i = -1$), or σ_i^{\pm} (matrix element between two states with opposite Z_i).

It can be checked that ρ_2 is separable at all times. We also checked that ρ_3 and ρ_4 (not shown) show no negativity, whatever the time t . Although the systems has some global multipartite entanglement (at least for sufficiently short times), the separability of reduced density matrices is a known property of graph states and GHZ states [15]. It is presumably the case at all times in the present model, unless one considers the system *globally* (all qubits).

4 Computational results

4.1 Dissipative dynamics of observables

In this section we present the dynamics of Pauli observables calculated from the analytic expressions of Eqs. 30-32, together with numerical simulation results from the MPO solver. In App. A we give more details on the numerical simulations of the density matrix dynamics. To explore the parameter space, we studied five representative cases varying the values of g_0 , g_1 and g_2 . The values used are shown in Tab. 1, together with some characterization of the environments that would produce such parameter values.

First, we look at Eq. 30 in the left panel of Fig. 1. The numerical results are in perfect agreement with the theory. Since the expectation value of a product of an odd number of Y vanishes, $\langle YY \rangle$ is a *connected* correlation, and it shows a decay with a characteristic timescale $\sim 1/\alpha$.

Now we turn to Eq. 31, first in a simple case for the single qubit observable $\langle Z \rangle$. The result is displayed in the right panel of Fig. 1 (this corresponds to $n = 0$ and $l = 1$). The cases 2 and 5 are not shown since they have $\gamma = 0$ and thus $\langle Z \rangle = 0$. $\langle Z \rangle$ displays a relaxation toward the steady state value $\langle Z \rangle_{t \rightarrow \infty} = \frac{\gamma}{\beta} = \frac{g_0 - g_1}{g_0 + g_1}$. When $g_1 = 0$ this is simply a relaxation toward

	Environment	g_0	g_1	g_2	α	β	γ
case 1	Spontaneous emission only	1	0	0	0.5	1	1
case 2	Pure dephasing	0	0	1	2	0	0
case 3	Low temperature, low dephasing	0.9	0.1	0.1	0.7	1	0.8
case 4	Generic dissipative rates	0.6	0.4	0.25	1	1	0.2
case 5	Infinite temperature with dephasing	1	1	1	3	2	0

Table 1: Different sets of physical parameters used in the simulations.

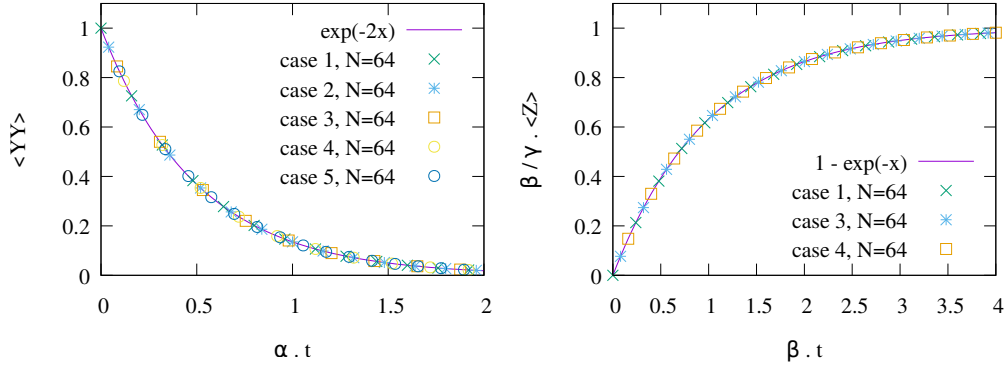


Figure 1: Left: Time evolution of $\langle YY \rangle$ in the different parameter cases with 64 qubits. The rescaled time $\alpha \cdot t$ in the horizontal axis allows the collapse of the curves associated to different sets of parameters. The line corresponds to Eq. 30 in the case $n = 1$. Right: same for $\langle Z \rangle$. For this quantity the relevant rescaling of the time is $\beta \cdot t$. The line corresponds to Eq. 31 in the case $n = 0$ and $l = 1$. Cases 2 and 5 are not shown as they have $\gamma = 0$ and thus $\langle Z \rangle = 0$.

the $|0\rangle$ state. We also note that effect of the correlations in the system are invisible in this observable, in the sense that the exact same behavior would be observed whatever the initial state provided that $\langle Z \rangle = 0$ on all qubits at time 0.

In the more complex case where $n \neq 0$, we cannot scale all the cases on one curve, so we chose to show the dependence in the number of qubits for one case. In the left panel of Fig. 2, we show the time evolution of $\langle YYZ \rangle$ (that is $n = 1$ and $l = 1$) for case 1 and different number of qubits. Again the simulations are in perfect agreement with the theory. This observable has a non-monotonous time evolution for a simple reason: from Eq. 31 we see this 3-point observable factorizes into $\langle YYZ \rangle = \langle YY \rangle \langle Z \rangle$, that is a product of a decreasing function by an increasing function. Cases 3 and 4 have similar behaviors, whereas cases 2 and 5 have $\gamma = 0$ and thus $\langle YYZ \rangle = 0$.

Finally, we also checked the expectation value of the stabilizer of the complete graph state, that is Eq. 32 with $n = 1$. The results are displayed in the right panel of Fig. 2, they are again in perfect agreement to the theory. The initial value is 1, as it should since the initial state is an eigenstate of the stabilizer for the eigenvalue 1. We then observe an exponential decay with a characteristic timescale given by $(\alpha + (N - 1)\beta)^{-1}$ and which decreases with the number of qubits. This size-dependence of the decay rate can be viewed as a consequence of the fact that this specific observable involves all the qubits and reflects some global correlations in the system.

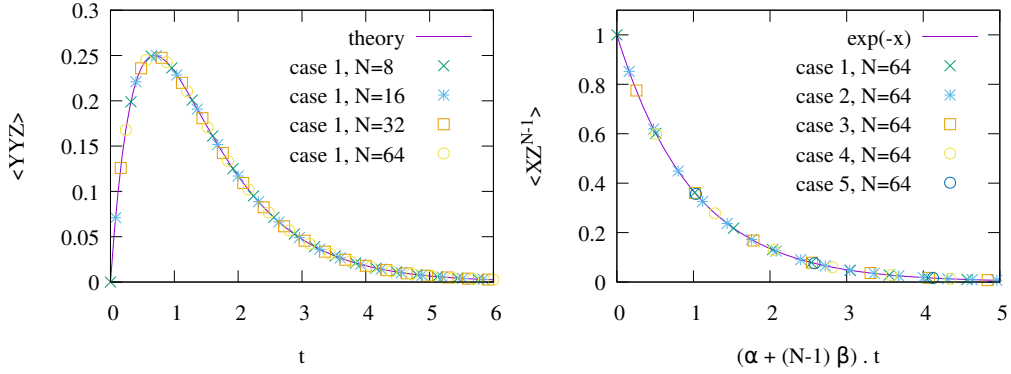


Figure 2: Left: Time evolution of $\langle YYZ \rangle$ for case 1 for different values of N . The line corresponds to Eq. 31 in the case $n = 1$ and $l = 1$. Cases 3 and 4 have similar behaviors, whereas cases 2 and 5 have $\gamma = 0$ and thus $\langle YYZ \rangle = 0$. As discussed in the text, the dynamics of this observable correspond to the product of two exponentials, making it nonmonotonous. Right: Time evolution of the stabilizer $\langle XZ^{N-1} \rangle$. The rescaled time in the horizontal axis ensures that the different simulations (cases 1, \dots , 5) fall onto the same curve, clearly showing the scaling of the β contribution of the decay rate with the system size. The line corresponds to Eq. 32 for $n = 1$.

4.2 Operator space entanglement entropy

The method to compute the von Neumann entanglement entropy associated to a given bipartition of a graph state is explained in Ref. [4]. In the case of the complete graph state the result is $S_{vN} = \ln 2$ whatever the bipartition (for two non-empty subsystems). This result is also easy to obtain using the fact that the complete graph state is LC-equivalent to the GHZ state.

For a mixed state ρ , it is interesting to consider the operator space entanglement entropy (OSEE) [27], a quantity that naturally arises in simulations of the density matrix dynamics represented using matrix product operators. It can be defined by considering the vectorization $|\rho\rangle\rangle$ of ρ , which is a pure state in an enlarged Hilbert of dimension 4 per site (spanned by the 3 Pauli matrices plus the identity matrix). The OSEE associated to a given bipartition into two subsystems A and B is by definition the von Neumann entanglement $\text{OSEE}^{AB} = S_{vN,|\rho\rangle\rangle}^{(A)} = S_{vN,|\rho\rangle\rangle}^{(B)}$ associated to this partition of the vectorized pure state $|\rho\rangle\rangle$. The OSEE quantifies the total amount of correlations between the two subsystems. We note also that the OSEE alone does not indicate whether the correlations are mostly classical or quantum.

For a pure state $|g\rangle$, the associated density matrix is $\rho = |g\rangle\langle g|$ and OSEE of ρ for a given bipartition is by construction twice the von Neumann entropy associated to the same bipartition in $|g\rangle$. So, in our model, the OSEE at time $t = 0$ is $2 \ln 2$ for any nontrivial bipartition of the N qubits. At long times the system reaches a product state (if $g_1 = 0$ it simply corresponds to all the qubits in state $|0\rangle$) which is a state with bond dimension equal to 1 and vanishing OSEE. At intermediate finite times $t > 0$, the OSEE must therefore decrease from its initial value and eventually converge to 0 for any bipartition of the system. It is, however, no longer independent of the bipartition and in the rest of the paper, we will focus of the bipartition in two subsystems of equal size ($N/2$).

The dynamics of the OSEE for this bipartition in two equal halves of system is shown in Fig. 3. The interesting feature is the appearance of a very clear plateau at $\text{OSEE} = \ln 2$, whose duration grows with the number of qubits.

To explore this behavior, we determined numerically the scaling laws for both the time at

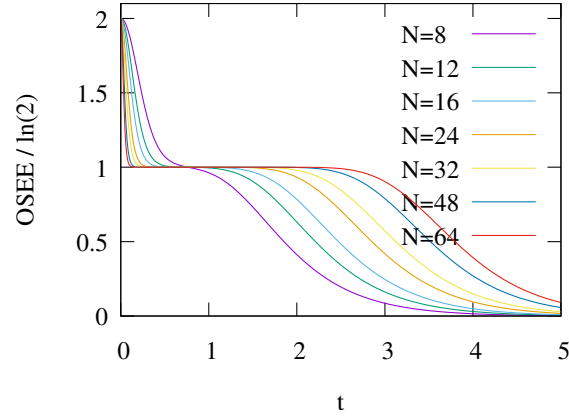


Figure 3: Time evolution of the OSEE between the two halves of the system for different number of qubits in case 1. A plateau in the OSEE value at intermediate times, whose duration grows (logarithmically) with the number of qubits is clear.

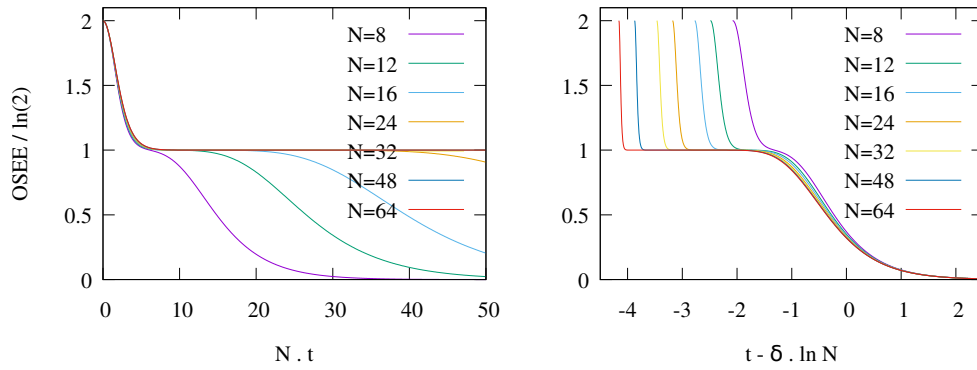


Figure 4: Time evolution of the OSEE between the two halves of the system for different values of N in case 1 (same data as Fig. 3). Left: time rescaled by a factor N . The collapse of the curves at early times shows that the initial drop of the OSEE takes place over a timescale proportional to $1/N$. Right: same data with time shifted by $\delta \ln N$, here $\delta = 1$. In this panel the collapse of the curves at the end of the plateau illustrates the fact that the duration of the plateau is proportional to $\delta \ln N$.

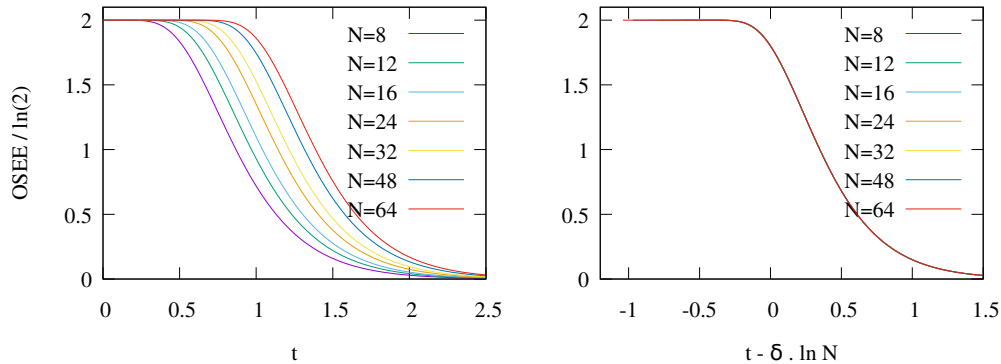


Figure 5: Time evolution of the OSEE between the two halves of the system for different number of qubits in case 2. Left: data plotted as a function of time. Right: data plotted as a function of time shifted by $\delta \ln N$, here $\delta = 0.25$. All the curves are essentially on top of one another and are indistinguishable at the scale of the figure.

which the plateau begins and the time at which it ends. We observe a $1/N$ behavior at early times and $\ln N$ behavior for the time at the end of the OSEE plateau. The corresponding plots are shown in Fig. 4. At early times, the behavior is similar for cases 3, 4 and 5 with a $1/N$ behavior (left panel Fig. 4) and a plateau at $\text{OSEE} = \ln 2$. Case 2 is different with a plateau that starts at $t = 0$, see Fig. 5. We suppose that this behavior is related to the fact that $\beta = 0$ in this case. At late times the $\ln N$ behavior seems universal, with different values of the prefactor δ (up to some finite size effects the OSEE depends only on $t - \delta \ln N$ at late times). In case 2, the data collapse is particularly striking (see right panel of Fig. 5).

Comparing the values of δ to the parameters in each case, we see that for all our cases the value of δ is compatible with $\delta = 1/(2\alpha)$. It is remarkable that the OSEE stays essentially constant for a duration that increases with the number of qubits, although the correlations decrease exponentially at best in constant time. A large enough system can be in a regime where $1/\beta \ll t$ and $t \lesssim \delta \ln(N)$. In case 1 (g_0 only) the first condition implies that $\langle Z \rangle$ is arbitrary close to 1, while the second condition puts the system in the OSEE plateau, with $\text{OSEE} \simeq \ln(2)$. In other words, the system can have an arbitrary low density of qubits in the $|1\rangle$ state and, still, some sizeable correlation between the two halves of the system.

We checked that such plateau is absent if the initial state is a graph state with a lower connectivity. As an example, Fig. 6 shows the OSEE in a case where the initial state is a graph state constructed from a periodic one-dimensional lattice with N sites (a ring). For a subsystem A of the form $A = [1, \dots, n]$ with $N - 2 \geq n \geq 2$ the von Neumann entanglement entropy is equal to $S_{\text{vN}}^A = 2 \ln(2)$ in a such ring graph state [4], hence the value $\text{OSEE} = 4 \ln(2)$ at time $t = 0$. The correlations are plausibly only short-ranged (with a finite correlation length) in that case, so that the correlations between the two halves of the bipartition essentially come from the qubits close to the boundaries/cutting between the two halves. Thus, when the system size becomes significantly larger than the correlation length the OSEE becomes independent of N . The OSEE then drops to zero over a characteristic timescale which is independent of the system size, contrary to the cases where the initial state is a complete graph.

5 Conclusion

In this paper we introduced an exactly solvable toy model for the decoherence of a graph state. We have considered the time evolution of the complete graph state under a Lindblad equation

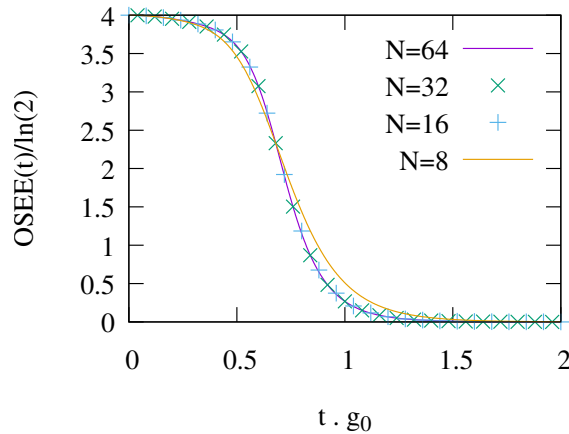


Figure 6: Time evolution of the OSEE between the two halves of the system, for a simulation of a *ring* graph state (initialized at $t = 0$), with the dissipator \mathcal{D}_0 . The data for $N = 16, 32$ and 64 are almost on top of each other, showing rapid convergence to a limiting curve in the large N limit. Contrary to the cases where the initial state is a complete graph, these curve do not exhibit any plateau. In this simulation the MPO bond dimension is 16 or below.

with general single-qubit dissipators and a vanishing Hamiltonian. Exploiting the permutation invariance of the model allowed obtaining simple closed formulae for the expectation values of any product of Pauli operators at any time. The method can in principle be extended to other types of graph states, although the number of equations will grow for less symmetric situations. The availability of analytic solutions would be valuable as a guiding tool in understanding the dissipative mechanisms acting in numerical studies of complex setups.

We have compared the theoretical results with a numerical solver that was pushed up to 64 qubits. The results are in perfect agreement with the theory, showing that the MPO approach is adapted for simulating this type of problem. MPO representations are often thought of as being appropriate for one-dimensional geometries, but the present example shows that it can also efficiently handle some problems with many qubits and in a high space dimension when the correlations are not too strong, as it is here.

A peculiar long-lasting plateau was identified in the OSEE between the two halves of the system, pointing to the presence of some nonlocal long-lived correlations (possibly classical) in this setup. Despite the dissipative processes acting everywhere on the qubits, the correlations are seen to survive for a time that increases with the system size. In a future study it would be interesting to compute exactly the OSEE to $t > 0$ in this model.

Acknowledgements

G.M. thanks Élie Gouzien for useful discussions about graph states, and is supported by the PEPR integrated project EPiQ ANR-22-PETQ-0007 part of Plan France 2030.

A Further simulation results

To encode ρ as an MPO, the bond dimension that one needs to use is closely related to the (exponential of the) OSEE. As mentioned above the initial state has $S_{vN} = \ln 2$ and $\text{OSEE} = 2 \ln 2$ for all bipartitions. As a pure state the initial state can be written exactly as a matrix-product state with bond dimension equal to 2, and as a density matrix ρ it can be represented exactly by an MPO of bond dimension equal to 4. It turns out that the effect of the dissipation does not increase the required bond dimension. The data indicate that an exact description of ρ is possible with a bond dimension equal to 4 in this model, even for $t > 0$. Note however that due to small numerical errors the bond dimension was sometimes observed to be above 4 in the simulations (but never exceeding 15). All the simulations used a time step $\tau = 0.004$.

References

- [1] H. J. Briegel and R. Raussendorf, *Persistent entanglement in arrays of interacting particles*, Phys. Rev. Lett. **86**, 910 (2001), doi:[10.1103/PhysRevLett.86.910](https://doi.org/10.1103/PhysRevLett.86.910).
- [2] R. Raussendorf and H. J. Briegel, *A one-way quantum computer*, Phys. Rev. Lett. **86**, 5188 (2001), doi:[10.1103/PhysRevLett.86.5188](https://doi.org/10.1103/PhysRevLett.86.5188).
- [3] R. Raussendorf, D. E. Browne and H. J. Briegel, *Measurement-based quantum computation on cluster states*, Phys. Rev. A **68**, 022312 (2003), doi:[10.1103/PhysRevA.68.022312](https://doi.org/10.1103/PhysRevA.68.022312).
- [4] M. Hein, J. Eisert and H. J. Briegel, *Multiparty entanglement in graph states*, Phys. Rev. A **69**, 062311 (2004), doi:[10.1103/PhysRevA.69.062311](https://doi.org/10.1103/PhysRevA.69.062311).
- [5] W. Dür, J. Calsamiglia and H.-J. Briegel, *Multipartite secure state distribution*, Phys. Rev. A **71**(4), 042336 (2005), doi:[10.1103/PhysRevA.71.042336](https://doi.org/10.1103/PhysRevA.71.042336).
- [6] N. Shammah, S. Ahmed, N. Lambert, S. De Liberato and F. Nori, *Open quantum systems with local and collective incoherent processes: Efficient numerical simulations using permutational invariance*, Phys. Rev. A **98**, 063815 (2018), doi:[10.1103/PhysRevA.98.063815](https://doi.org/10.1103/PhysRevA.98.063815).
- [7] P. Migdał, J. Rodriguez-Laguna and M. Lewenstein, *Entanglement classes of permutation-symmetric qudit states: Symmetric operations suffice*, Phys. Rev. A **88**, 012335 (2013), doi:[10.1103/PhysRevA.88.012335](https://doi.org/10.1103/PhysRevA.88.012335).
- [8] P. Espoukeh and P. Pedram, *Quantum teleportation through noisy channels with multi-qubit ghz states*, Quantum information processing **13**(8), 1789 (2014), doi:[10.1007/s11128-014-0766-2](https://doi.org/10.1007/s11128-014-0766-2).
- [9] D. C. Brody, L. P. Hughston and D. M. Meier, *Fragile entanglement statistics*, J. Phys. A Math. Theor. **48**(42), 425301 (2015), doi:[10.1088/1751-8113/48/42/425301](https://doi.org/10.1088/1751-8113/48/42/425301).
- [10] Y. Zhao, R. Zhang, W. Chen, X.-B. Wang and J. Hu, *Creation of greenberger-horne-zeilinger states with thousands of atoms by entanglement amplification*, NPJ Quantum Information **7**(1), 24 (2021), doi:[10.1038/s41534-021-00364-8](https://doi.org/10.1038/s41534-021-00364-8).
- [11] K. X. Wei, I. Lauer, S. Srinivasan, N. Sundaresan, D. T. McClure, D. Toyli, D. C. McKay, J. M. Gambetta and S. Sheldon, *Verifying multipartite entangled greenberger-horne-zeilinger states via multiple quantum coherences*, Phys. Rev. A **101**, 032343 (2020), doi:[10.1103/PhysRevA.101.032343](https://doi.org/10.1103/PhysRevA.101.032343).

- [12] G. J. Mooney, G. A. White, C. D. Hill and L. C. Hollenberg, *Generation and verification of 27-qubit greenberger-horne-zeilinger states in a superconducting quantum computer*, J. Phys. Commun. **5**(9), 095004 (2021), doi:[10.1088/2399-6528/ac1df7](https://doi.org/10.1088/2399-6528/ac1df7).
- [13] S. Moses, C. Baldwin, M. Allman, R. Ancona, L. Ascarrunz, C. Barnes, J. Bartolotta, B. Bjork, P. Blanchard, M. Bohn *et al.*, *A race track trapped-ion quantum processor*, arXiv:2305.03828 (2023), doi:[10.48550/arXiv.2305.03828](https://doi.org/10.48550/arXiv.2305.03828).
- [14] W. Dür and H.-J. Briegel, *Stability of Macroscopic Entanglement under Decoherence*, Phys. Rev. Lett. **92**(18), 180403 (2004), doi:[10.1103/PhysRevLett.92.180403](https://doi.org/10.1103/PhysRevLett.92.180403).
- [15] M. Hein, W. Dür, J. Eisert, R. Raussendorf, M. Van den Nest and H.-J. Briegel, *Entanglement in graph states and its applications*, In *Quantum Computers, Algorithms and Chaos*, pp. 115–218. IOS Press, doi:[10.3254/978-1-61499-018-5-115](https://doi.org/10.3254/978-1-61499-018-5-115) (2006).
- [16] O. Gühne, F. Bodoky and M. Blaauuboer, *Multipartite entanglement under the influence of decoherence*, Phys. Rev. A **78**(6), 060301 (2008), doi:[10.1103/PhysRevA.78.060301](https://doi.org/10.1103/PhysRevA.78.060301).
- [17] D. Cavalcanti, R. Chaves, L. Aolita, L. Davidovich and A. Acín, *Open-System Dynamics of Graph-State Entanglement*, Phys. Rev. Lett. **103**(3), 030502 (2009), doi:[10.1103/PhysRevLett.103.030502](https://doi.org/10.1103/PhysRevLett.103.030502).
- [18] G. Lindblad, *On the generators of quantum dynamical semigroups*, Commun. Math. Phys. **48**(2), 119 (1976), doi:[10.1007/BF01608499](https://doi.org/10.1007/BF01608499).
- [19] V. Gorini, A. Kossakowski and E. C. G. Sudarshan, *Completely positive dynamical semigroups of N-level systems*, J. Math. Phys. **17**(5), 821 (1976), doi:[10.1063/1.522979](https://doi.org/10.1063/1.522979).
- [20] H. Landa and G. Misguich, *Nonlocal correlations in noisy multiqubit systems simulated using matrix product operators*, SciPost Phys. Core **6**, 037 (2023), doi:[10.21468/SciPostPhysCore.6.2.037](https://doi.org/10.21468/SciPostPhysCore.6.2.037).
- [21] github.com/qiskit-community/lindbladmpo.
- [22] M. Fishman, S. White and E. Stoudenmire, *The ITensor Software Library for Tensor Network Calculations*, SciPost Physics Codebases p. 004 (2022), doi:[10.21468/SciPostPhysCodeb.4](https://doi.org/10.21468/SciPostPhysCodeb.4).
- [23] H. Weimer, A. Kshetrimayum and R. Orús, *Simulation methods for open quantum many-body systems*, Rev. Mod. Phys. **93**(1), 015008 (2021), doi:[10.1103/RevModPhys.93.015008](https://doi.org/10.1103/RevModPhys.93.015008).
- [24] A. McDonald and A. A. Clerk, *Exact solutions of interacting dissipative systems via weak symmetries*, Phys. Rev. Lett. **128**, 033602 (2022), doi:[10.1103/PhysRevLett.128.033602](https://doi.org/10.1103/PhysRevLett.128.033602).
- [25] D. M. Greenberger, M. A. Horne and A. Zeilinger, *Going Beyond Bell's Theorem*, In M. Kafatos, ed., *Bell's Theorem, Quantum Theory and Conceptions of the Universe*, Fundamental Theories of Physics, pp. 69–72. Springer Netherlands, Dordrecht, ISBN 978-94-017-0849-4, doi:[10.1007/978-94-017-0849-4_10](https://doi.org/10.1007/978-94-017-0849-4_10) (1989).
- [26] H.-P. Breuer and F. Petruccione, *The Theory of Open Quantum Systems*, Oxford University Press, ISBN 9780199213900, doi:[10.1093/acprof:oso/9780199213900.001.0001](https://doi.org/10.1093/acprof:oso/9780199213900.001.0001) (2007).
- [27] T. Prosen and I. Pižorn, *Operator space entanglement entropy in a transverse Ising chain*, Phys. Rev. A **76**(3), 032316 (2007), doi:[10.1103/PhysRevA.76.032316](https://doi.org/10.1103/PhysRevA.76.032316).